# Development and validation of an analytical pyrolysis method for detection of airborne polystyrene nanoparticles

Freja Hasager, Þuríður N. Björgvinsdóttir, Sofie F. Vinther, Antigoni Christofili, Eva R. Kjærgaard, Sarah S. Petters, Merete Bilde, Marianne Glasius [*]

*Department of Chemistry, Aarhus University, Langelandsgade 140, 8000, Aarhus, Denmark*

A B S T R A C T

Microplastic is ubiquitous in the environment. Recently it was discovered that microplastic (MP, 1 μm−5 mm) contamination is present in the atmosphere where it can be transported over long distances and introduced to remote pristine environments. Sources, concentration levels, and transportation pathways of MP are still associated with large uncertainties. The abundance of atmospheric MP increases with decreasing particle size, suggesting that nanoplastics (NP, < 1 μm) could be of considerable atmospheric relevance. Only few analytical methods are available for detection of nanosized plastic particles. Thermoanalytical techniques are independent of particle size and are thus a powerful tool for MP and NP analysis. Here we develop a method for analysis of polystyrene on the nanogram scale using pyrolysis gas chromatography coupled to mass spectrometry. Pyrolysis was performed using a slow temperature ramp, and analytes were cryofocused prior to injection. The mass spectrometer was operated in selected ion monitoring (SIM) mode. A lower limit of detection of $1 \pm 1$ ng and a lower limit of quantification of $2 \pm 2$ ng were obtained (for the trimer peak). The method was validated with urban $PM_{2.5}$ matrices of low (7 μg per sample) and high (53 μg per sample) aerosol mass loadings. The method performs well for low $PM_{2.5}$ loadings, whereas high $PM_{2.5}$ loadings seem to cause a matrix effect reducing the signal of polystyrene. This effect can be minimized by introducing a thermal desorption step prior to pyrolysis. The study provides a novel analysis method for qualitative and semi-quantitative analysis of PS on the nanogram scale in an aerosol matrix. Application of the method can be used to obtain concentration levels of polystyrene in atmospheric MP and NP. This is important in order to improve the understanding of the sources and sinks of MP and NP in the environment and thereby identify routes of exposure and uptake of this emerging contaminant.

## 1. Introduction

Plastic pollution is widely distributed in the environment and is present in all environmental compartments. Microplastics (MP) are solid plastic particles with diameters ranging from 5 mm down to 1 μm and nanoplastics (NP) are plastic particles with diameters in the sub-micrometer range. MP is directly emitted to the environment from, e.g., personal care products (primary MP), or formed in the environment from weathering of macroplastics (secondary MP) [1–3]. Microplastic particles are present in oceans [4], rainwater [5], freshwater, sediment [6], soil [7], polar ice [8], wildlife [9] and in the human body [10,11]. The presence of MP in the human body is associated with adverse health effects [12], and the presence of MP in the environment could have

implications for ecosystem health [13]. In recent years it has become apparent that MP pollution is present in the atmosphere [14], where it can be transported over long distances [15,16]. Airborne MP has been observed in indoor [14,17], urban [14,18,19], continental, remote [20], and marine air [21–23] as well as in the free troposphere [16,24]. The dominant source of MP in the air is populated urban areas. Indoor MP concentrations can exceed outdoor concentrations [17], while urban MP concentrations exceed sub-urban [14] and remote MP concentrations [20]. Traffic emits MP from wear of tires and brakes [25], and by resuspension of deposited MP [26]. The ocean also acts as a source and sink of atmospheric MP [23,27]. Atmospheric MP can have implications for climate through radiative effects [28], degradation products [29], and by affecting precipitation [30] and cloud formation processes [31].

* Corresponding author.
*E-mail address:* glasius@chem.au.dk (M. Glasius).

The lower size limit for detection of MP particles is limited by the analytical method. The most frequently used methods for environmental MP analysis include microscopy, Fourier transform infrared (FTIR), and Raman spectroscopy [32], with a lower size limit of 2 μm [33]. Only few analytical methods are available for the detection of NP [34–36]. Several studies show that the number concentration of airborne MP increases with decreasing particle size [14–16,20], suggesting that NP could be of considerable atmospheric and health relevance [37]. NP has been observed in snow in the remote high-altitude Alps [38], and in ice/firn core samples from the Arctic and Antarctic [8]. Concentrations of airborne MP are reported in several different units depending on the sampling and analytical methods, including particles per $m^3$ of air, deposited particles per $m^2$ per day, mg of MP per kg of dust, and particles per L of melted snow [39]. This renders it difficult to compare concentrations of airborne MP across studies. For particulate matter (PM) suspended in air, it is customary to report concentrations in units of mass. Mass concentration of MP and NP can be determined with thermoanalytical methods, as these depend on the mass of MP and NP and are independent of particle size.

Pyrolysis gas chromatography coupled to mass spectrometry (py-GC-MS) is a well established analytical method for polymers in the plastic industry, and has also proven applicable for detection of MP in environmental samples [40–42]. Py-GC-MS can be used to determine polymer types, and is mainly limited by the sample mass. During pyrolysis the sample is heated under oxygen-free conditions, where the polymer is fragmented into smaller molecules that can enter the gas phase and be analyzed with a gas chromatograph. When pyrolysis conditions are held constant, the resulting pyrogram (chromatogram obtained from pyrolysis) will function as a fingerprint of a specific polymer. Tsuge et al. provides an extensive data book of pyrograms of synthetic polymers at a pyrolysis temperature of 600 °C [43]. Complex environmental samples can contain several polymers simultaneously along with organics from the sample matrix which can result in formation of secondary pyrolysis products, creating additional peaks in the pyrograms compared to the pure polymers [44]. The most commonly used pyrolysis method is flash pyrolysis, where the sample is heated instantly (10-20 s) yielding a mix of hot vapors that can recombine to form secondary products. A novel approach to decrease secondary product formation has recently been suggested, where a slow ramping of the pyrolysis temperature is chosen instead of flash [45]. Thereby, the vapors are formed and removed continuously in the pyrolysis unit, reducing the mix of hot vapors, and hence minimizing the formation of secondary products. Py-GC-MS serves as a promising method for analysis of MP in complex atmospheric samples and allows for reporting mass concentrations comparable to PM measurements typically done in air pollution studies.

Globally, 25 mega tonnes of polystyrene (PS) were produced in 2015, a number that is increasing each year [46]. PS is mainly used for packaging, building/construction, and consumer products. Of the 25 mega tonnes, only 17 mega tonnes were recycled. The remaining PS is either still in use or accumulating in landfills or the environment [46]. Microparticles of PS have been detected in the atmosphere [15,16,23,24,47], and especially low-density ($\rho < 0.1$ g $cm^{-3}$) PS has the potential for long-range atmospheric transport.

Here we have developed a novel py-GC-MS analysis method for identification and quantification of PS on the nanogram scale. The method was validated with respect to an urban $PM_{2.5}$ matrix of low (7 μg per sample) and high (53 μg per sample) aerosol mass loadings. Two types of PS were considered: expanded polystyrene ($\rho < 0.04$ g $cm^{-3}$), and 800 nm polystyrene latex spheres ($\rho = 1.05$ g $cm^{-3}$). The aim of the study is to develop a method that will enable the determination of concentration levels of this emerging contaminant, which is an important part of understanding the extent of the atmospheric MP issue, along with transport pathways and exposure routes.

## 2. Experimental

### 2.1. Materials

Polystyrene latex (PSL) nanospheres of sizes $81 \pm 3$ nm, and $803 \pm 14$ nm were obtained from Thermo Scientific™ 3000 Series Nanospheres™ Size Standards with a concentration of 1% solids in water (Fremont, CA, USA). The PSL suspension contains sodium azide as a preservative and a sulfate-based surfactant. Expanded polystyrene (ePS) were obtained from Jackopor® (> 98 wt% PS and < 2 wt% mixed pentane isomers, BEWI, Trondheim, Norway). Chloroform (99.80%, HiPerSolv, VWR Chemicals, Leuven, Belgium) and MilliQ water (<0.05 μS $cm^{-1}$ at 25 °C) were used for preparation of standards. Open-ended quartz pyrolysis tubes (Gerstel, Mülheim, Germany) were used to minimize the risk of carry-over contamination [48].

### 2.2. Sample preparation

Standards were prepared by packing an open-ended pyrolysis tube with quartz wool and adding 1-3 μL of a PSL or ePS standard solution. Tubes were left under a cover of aluminum foil overnight to allow evaporation of water or for 30 min to allow chloroform evaporation leaving only PSL or ePS in the sample tube. Plastic contamination during the experimental procedure was minimized by wearing cotton laboratory coats, storing quartz wool in glass vials, and storing cleaning reagents (MilliQ, ethanol, and acetone) in glass containers. A syringe of metal and glass (Gerstel, 10 μl) was used to measure and transfer standards to the pyrolysis tubes. Quartz wool, pyrolysis tubes and metal equipment used during the sample preparation were cleaned by heating to 1100 °C using a butane gas burner (Cook & Baker). Aluminum foil was used to cover the table workspace during sample preparation to ensure clean conditions. Instrumental and procedural blanks were run to test for background contamination. Five standard solutions of 803 nm PSL in MilliQ were prepared by serial dilution with concentrations of 1.4, 3.5, 8.6, 22, and 54 ng μL$^{-1}$. PSL standards in the 1-160 ng mass range were prepared from the standard solutions by adding 1-3 μL of PSL standard and evaporating the water. PSL solutions were gently mixed and sonicated for 10 s prior to use. Five standard solutions of ePS in chloroform were prepared by serial dilution with concentrations of 1.1, 5, 10, 20, and 55 ng μL$^{-1}$, and used to prepare ePS standards with masses in the 1-110 ng range.

### 2.3. Instrumentation

Analyses were performed with a pyrolysis module (PYRO Gerstel) connected to a thermal desorption unit (TDU Gerstel, from now on referred to as TDU) and cooled injection system (CIS4 Gerstel, from now on referred to as CIS). The pyrolysis module, TDU, and CIS were interfaced with a gas chromatograph coupled to a mass spectrometer (7890b and 5977a Agilent Technologies, respectively). Pyrolysis was performed as a slow temperature ramping from 300 °C to 800 °C at 5 °C s$^{-1}$. During pyrolysis the TDU was heated from 40 °C to 300 °C at 300 °C min$^{-1}$ and held for 2 min at 300 °C. Pyrolysis fragments were transferred to the CIS liner in splitless mode by a constant flow of helium of 50 mL min$^{-1}$, and cryofocused by cooling the CIS to temperatures ranging between −120 °C and −40 °C. During transfer, the TDU transfer temperature was set to 320 °C, however, the temperature proved to be unstable and would decrease to below 180 °C over a time scale of < 4 min. The instability was consistent and is thus not expected to cause variations in the data. Pyrolyzates were introduced at a constant helium flow of 1 mL min$^{-1}$ to the fused silica capillary GC column (HP-5MS Ultra Inert, 30 m × 0.25 mm inner diameter × 0.25 μm film thickness) by heating the CIS to 325 °C at 12 °C s$^{-1}$ with a total split ratio ranging between 20:1 and 75:1. The GC oven temperature was set at 40 °C, held for 2 min, and ramped to 320 °C at 10 °C min$^{-1}$ and then held for

5 min. The MS was operated at 70 eV electron ionization with the electron source at 250 °C, and the quadrupole at 150 °C. The MS was run in either scan or selected ion monitoring (SIM) mode. In the initial method the CIS temperature was set to −120 °C, the CIS split ratio to 75:1, and the MS scanned in the 10-550 mass-to-charge (m/z) range.

### 2.4. Method optimization

Relative to the initial method the following parameters were optimized i) the CIS temperature, ii) the CIS split ratio, iii) the scan range of the MS, and iv) the dwell time of selected ions in the SIM mode. The effect of the CIS temperature was investigated by testing 5 different temperatures: -120 °C, −100 °C, −80 °C, −60 °C, and −40 °C. The effect was evaluated based on peak area, signal-to-noise ratio (SNR), and symmetry factor calculated as the leading and trailing half-widths of the peak. Next, the CIS temperature was held constant at the optimized value, while the CIS split ratios 75:1, 50:1, 35:1 and 20:1 were tested. The optimized split ratio was identified and held constant while the MS was operated in SIM mode. The MS scanned in three sections during the run: section 1 at retention time (RT) 3-12 min for the styrene monomer marker ions with m/z of 51.1, 78.1, 104.1, section 2 at RT 12-22 min for the styrene dimer marker ions 91, 104, 130 m/z, and section 3 at RT 22-35 min for the styrene trimer marker ions 91, 117, 312 m/z. Three SIM methods with varying dwell times were tested: 70 ms (SIMA), 100 ms (SIMB), and 150 ms (SIMC).

### 2.5. Method validation

Calibration curves were constructed for the final optimized method, and the limit of detection (LOD) and limit of quantification (LOQ) were calculated from SNR, where the LOD is at SNR = 3, and the LOQ is at SNR = 10 [49].

Ambient aerosol particles were collected in Aarhus, Denmark (56° 10'N, 10° 12'E), using a high-volume aerosol sampler (Digitel DHA-80) equipped with a $PM_{2.5}$ inlet. Particles were collected onto 15 cm pre-baked (600 °C for 4 hours) quartz fiber filters with a flow rate of 500 L min$^{-1}$. Two particle filter samples were collected: One that was sampled for 7 days from March 21 11:10 to March 28 2022 11:10, and another that was sampled for 3 days from March 28 11:20 to March 31 12:04 2022. The average $PM_{2.5}$ concentration in Aarhus (measured at the street station Banegårdsgade) between March 21-28 was $26 \pm 13$ µg m$^{-3}$ (mean ± standard deviation), and $8 \pm 3$ µg m$^{-3}$ between March 28-31 [50], resulting in aerosol mass loadings of $53 \pm 21$ µg per filter punch-out for the first sampling period, and $7 \pm 3$ µg per punch-out for the second period. Weather conditions for the two sampling periods were similar with respect to relative humidity (72 ± 5%), temperature (5 ± 2 °C), wind speed (3 ± 1 m s$^{-1}$) and precipitation (0 mm) [51]. Filters were packed in aluminum foil and stored at −18 °C until analysis. Punch-outs of 3 mm were taken in duplicate from the blank filters and in triplicate from the sample filters. Sample filters were spiked with 20 and 60 ng ePS. A quality control of 60 ng ePS on a clean filter punch-out was included.

Additional tests of PS recovery from filters treated with MilliQ water and salt traces (Cl, Na, $SO_4$, Mg, K, Ca) were performed to assess if general handling of filters in the laboratory could lead to contamination influencing the analysis.

### 2.6. Data analysis

Data analysis was done using Agilent MassHunter Quantitative Analysis (version 10.1.733.0) and MassHunter Qualitative Analysis (version 10.0.1035.0). Further data processing was performed in MATLAB (R2021a) [52]. Mass spectra were matched against the NIST17 database, as well as a custom-built mass spectral library created using MassHunter Library Editor (version 10.1.733.0).
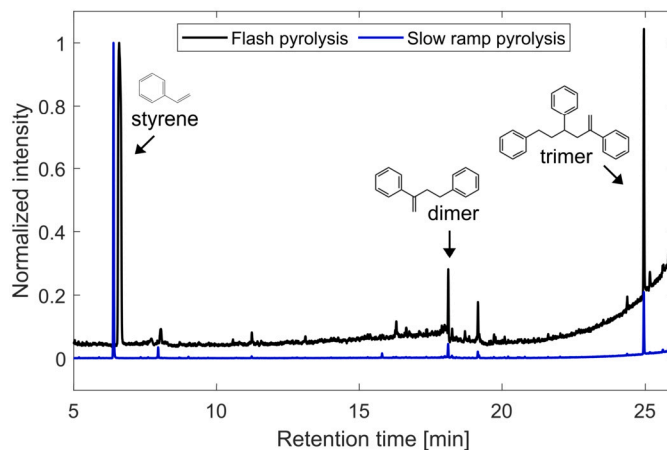


**Fig. 1.** PS pyrograms for the 50-312 m/z range obtained from flash pyrolysis at 500 °C (black line) and slow ramp pyrolysis 300-800 °C at 5 °C s$^{-1}$ (blue line) for 370 ng of 80 nm PSL standards. Intensities are normalized to styrene. (For interpretation of the colors in the figures, the reader is referred to the web version of this article.)

### 2.7. Uncertainty estimates

Standards used for the method optimization were only analyzed once. The uncertainty on these standards was calculated based on the standard deviation of five replicates of 84 ng 800 nm PSL standards. This standard deviation encompasses the variability of the sample preparation procedure together with the variability in analysis conditions. Calibration standards were run in duplicate and filter samples were run in triplicate. The reported uncertainties for the LOD and LOQ were determined from the standard deviation of 7 replicates of 10.4 ng 800 nm PSL and ePS standards.

Uncertainties reported for the PS masses from the two validation studies were propagated based on the standard deviations of the replicate measurements of the blanks and samples, as well as the standard error on the regression parameters from the calibration curves.

## 3. Results and discussion

Under the current conditions, polystyrene fragments into three major products during pyrolysis: the styrene monomer, styrene dimer (3-butene-1,3-diyldibenzene) and styrene trimer (5-hexene-1,3,5-triyltribenzene). The relative abundance of these three pyrolyzates depends on the pyrolysis temperature. At 500 °C pyrolysis the relative abundance is 1:0.25:1 (styrene:dimer:trimer) calculated from the peak intensities. At 600 °C the relative abundance is 1:0.25:0.5 (styrene:dimer:trimer) [43], and at 700 °C the relative abundance is 1:0.07 (styrene:dimer, trimer not observed) [40]. Thermal decomposition of PS occurs via inter- and intramolecular reactions [53,54]. Formation of secondary pyrolysis products can be minimized using slow temperature ramping during pyrolysis followed by cryotrapping prior to injection [45]. Fig. 1 shows pyrograms of PS from flash pyrolysis (500 °C) and slow ramp pyrolysis (300-800 °C at 5 °C s$^{-1}$) are shown. The dimer and trimer are less abundant during slow ramp pyrolysis compared to flash pyrolysis, with relative abundances of 1:0.05:0.2 (styrene:dimer:trimer). This intensity decrease is likely due to the suppression of the intermolecular formation pathway of the styrene dimer and trimer.

### 3.1. Cooled injection system temperature

Fig. 2 shows the peak area, symmetry factor and SNR as a function of the CIS temperature for the styrene monomer, dimer and trimer peaks for PSL standards of 80 nm (148 ng) and 800 nm (154 ng). For styrene, no clear trend is observed for the peak areas and at all temperatures, similar peak areas are obtained (panel A). There is a slight variation
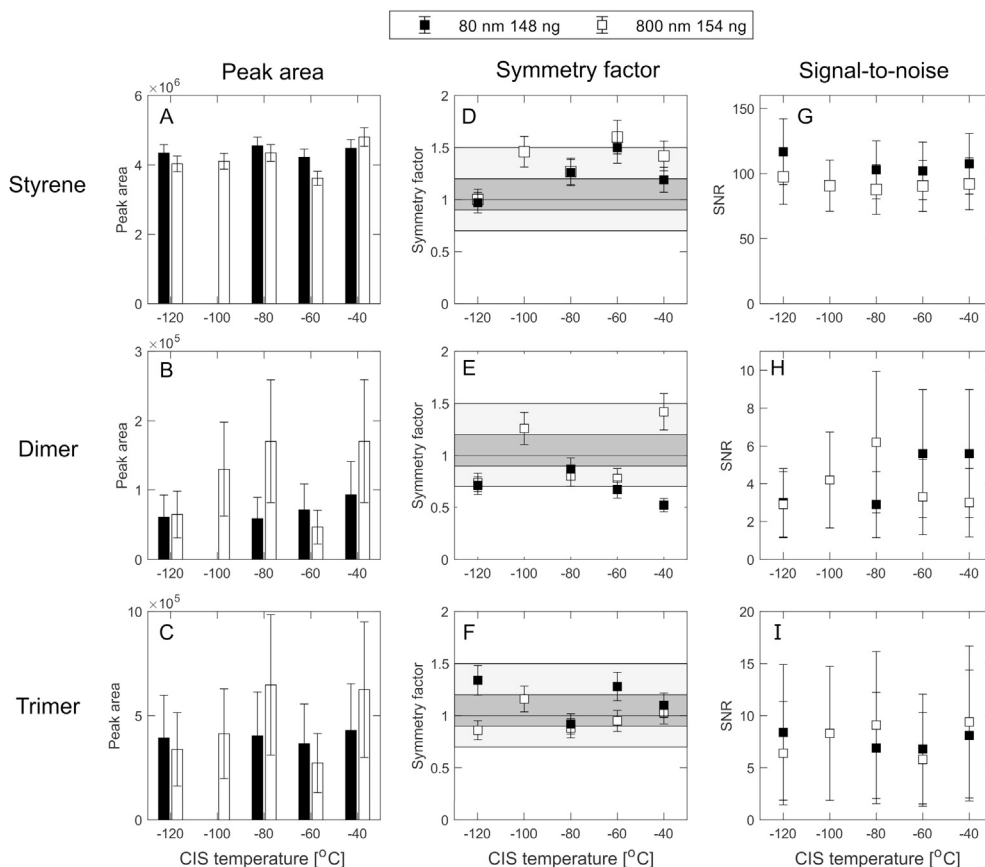
**Fig. 2.** Peak areas (left vertical panels, A-C), symmetry factors (center vertical panels, D-F), and signal-to-noise ratios (right vertical panels, G-I) for the styrene monomer (upper horizontal panels), dimer (center horizontal panels) and trimer (lower horizontal panels) obtained at different CIS temperatures. Black denotes 148 ng 80 nm PSL and white denotes 154 ng 800 nm PSL. Split ratio was 75:1. For CIS temperature of −100 °C no sample for 80 nm PSL particles was run. Dark shading indicates the acceptable symmetry range, and light shading indicates the limits of tailing and fronting according to Meyers et al. [55].

observed for the two PSL masses of 148 ng and 154 ng, however, this is not expected to be due to the 6 ng difference, but instead due to small variations in analysis conditions or sample preparation. Peak areas for the styrene dimer (panel B) and trimer (panel C) follow no clear trend as a function of CIS temperature. This is expected to be due to the low intensity and low SNR, rendering the dimer and trimer peaks sensitive to small variations in analysis conditions and sample preparation.

The styrene peak (panel D) is symmetric at a CIS temperature of −120 °C and asymmetric for the other temperatures. Peaks with symmetry factors between 0.9 and 1.2 are considered symmetric, while tailing results in values above 1.5 and fronting in values below 0.7 [55]. At −80 °C, the two PSL sizes give consistent values of the symmetry factor just outside of the acceptable range, while at −40 °C the two PSL sizes give inconsistent values for the symmetry factor, however, the 800 nm 154 ng PSL sample is within the symmetric range. At a CIS temperature of −100 °C the symmetry factor is near the tailing limit, and at −60 °C it is above.

For the dimer peak, symmetry factors (panel E) obtained at CIS temperatures of −100 °C and −80 °C are within the acceptable range, while symmetry factors obtained at other temperatures lie outside of the acceptable range. This is likely due to the small peak intensity and low SNR, causing small variations in e.g. sample preparation or analysis conditions to induce large variations in the chromatographic peak.

The trimer peak (panel F) is symmetric at CIS temperatures of −40 °C, −80 °C and −100 °C. At −60 °C the trimer peak is somewhat symmetric, as the 800 nm standard lies outside of the symmetric range, while the 80 nm standard lies within the acceptable range.

SNRs for the styrene peak (panel G) generally lie around 100 and the styrene peak is thus well suited for both qualification and quan-

tification. The dimer peak is close to the noise limit with SNR values of 3-6 (panel H). SNRs for the trimer peak are above 5 for all temperatures (panel I).

Cooling of the CIS adds several minutes to the analysis time, thus a relatively high cryofocusing temperature is preferred. The unstable TDU transfer temperature could be due to the large temperature difference between the CIS and the TDU transfer line (320 °C), hence a high cryofocusing temperature would minimize this difference and perhaps the instability of the TDU transfer temperature. Based on the symmetry factors, peak areas, and analysis time considerations, an optimal CIS temperature of −40 °C was chosen in the current study, yet −80 °C could also be applied.

### 3.2. Cooled injection system split ratio

The split ratio of the cooled injection system controls the amount of analyte transferred from the CIS to the column. Here, four different split ratios of 75:1, 50:1, 35:1, and 20:1 were tested for 800 nm PSL standards of 162 ng. Fig. 3 shows the peak areas, symmetry factors, and SNRs for the styrene monomer, dimer, and trimer as a function of split ratio.

The peak area of styrene (panel A) increases, as expected, as a function of split ratio. Areas for split ratios of 20:1-50:1 are similar within the uncertainties. Split ratios 75:1 and 35:1 yield tailing peaks (panel D), and split ratios 50:1 and 20:1 yield symmetry factors below 1.5. SNRs for styrene (panel G) lie in the range of 35-135, with split ratio 35:1 giving the highest SNR and split 50:1 giving the lowest SNR. For the dimer and trimer, peak areas (panels B and C) along with SNR (panels H and I) increase exponentially with decreasing split ratio. Split ratios 35:1 and 20:1 yield symmetric peaks (panels E and F), while split
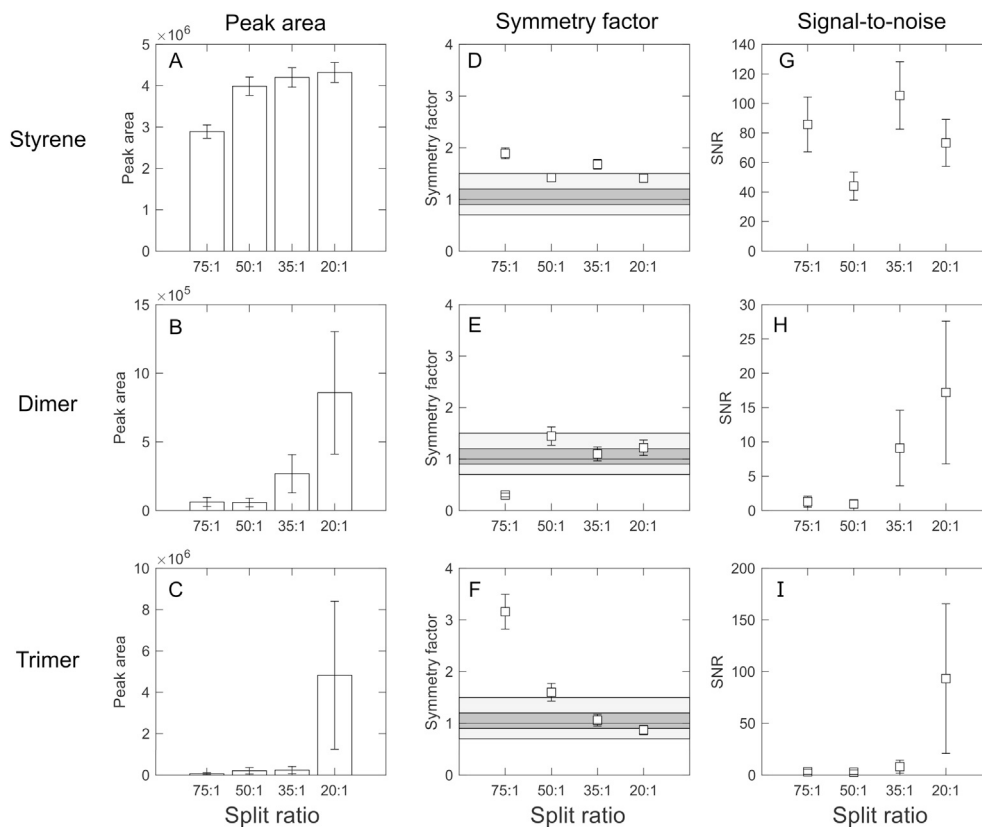
**Fig. 3.** Peak areas (left vertical panels, A-C), symmetry factors (center vertical panels, D-F) and signal-to-noise ratios (right vertical panels, G-I) for the styrene monomer (upper horizontal panels), dimer (center horizontal panels), and trimer (lower horizontal panels) obtained at different CIS split ratios for 162 ng 800 nm PSL standards. In the center panels, dark shading indicates the acceptable symmetry range, and light shading indicates the limits of tailing and fronting according to Meyers et al. [55].

**Table 1**
Signal-to-noise ratios obtained from the scan method given as total ion chromatogram (TIC) and extracted ion chromatogram (EIC), along with the three SIM methods for the styrene, dimer, and trimer peaks. Obtained from 162 ng 800 nm PSL standards.

|  | TIC | EIC | SIMA | SIMB | SIMC |
|---|---|---|---|---|---|
| **Styrene** | $44 \pm 10$ | $1081 \pm 234$ | $(25 \pm 6) \cdot 10^3$ | $(26 \pm 6) \cdot 10^3$ | $(20 \pm 4) \cdot 10^3$ |
| **Dimer** | $1 \pm 0.6$ | $8 \pm 5$ | $231 \pm 140$ | $614 \pm 371$ | $711 \pm 430$ |
| **Trimer** | $3 \pm 2$ | $101 \pm 79$ | $353 \pm 274$ | $641 \pm 497$ | $623 \pm 483$ |

50:1 results in peaks on the border of tailing. Split 75:1 yields a fronting dimer peak (panel E), and tailing trimer peak (panel F). Decreasing the split ratio increases the total number of peaks in the chromatogram. Split 75:1 results in 23 peaks, split 50:1 in 50 peaks, split 35:1 in 80 peaks and split 20:1 in 102 peaks. A small number of peaks is preferred, as only the styrene monomer, dimer and trimer peaks are of interest.

Based on this analysis, an optimal split ratio of 50:1 was chosen. This split ratio is the best compromise between peak area, symmetry, SNR, and the total number of chromatographic peaks. It provides high styrene peak areas and SNR, and low peak areas and SNR for the dimer and trimer peaks. However, the latter is improved in the SIM method development.

### 3.3. Selected ion monitoring

The SIM method was developed to increase sensitivity and minimize noise. Table 1 lists the SNRs of the styrene monomer, dimer, and trimer peaks obtained from the scan method, for both the total ion chromatogram (TIC) and extracted ion chromatogram (EIC), and the three

SIM methods. It is evident from Table 1, that a higher sensitivity is obtained from the SIM mode compared to the scan mode. The SNR of styrene increases by a factor 25 going from the TIC to EIC, and factor of 500-700 going from EIC to SIM. For the dimer peak, the SNR increases a factor of 8 from the TIC to EIC, and a factor of 30-90 from EIC to SIM. The trimer SNR increases with a factor of 35 from TIC to EIC, and a factor 3-6 from EIC to SIM. Hence, the signal is significantly improved in the SIM mode compared to the scan mode.

Three SIM methods with varying dwell times were tested: 70 ms (SIMA), 100 ms (SIMB), and 150 ms (SIMC). The dwell time is the amount of time the MS spends recording a single ion. It is related to the SIM cycle time, and thereby to the number of data points across a peak. Generally, 10 or more data points are needed to properly describe a gas chromatographic peak [56]. Long dwell times reduce noise, however, the analytical signal can be averaged out if the dwell time is too long. Short dwell times accurately follow the analytical signal, but the associated noise is also recorded [57]. Additionally, long dwell times will result in a long cycle time, and thereby in few data points per peak, while short dwell times yield short cycle times and, hence, many data points per peak.
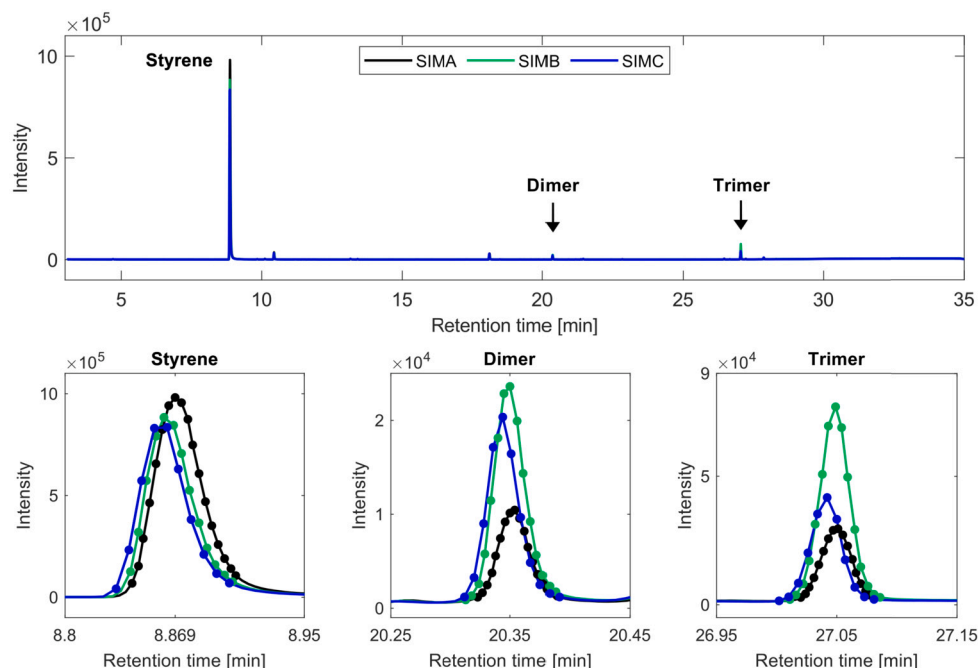
**Fig. 4.** Chromatograms obtained from the SIM methods for 162 ng 800 nm PSL standards. SIMA (black, 70 ms), SIMB (green, 100 ms), and SIMC (blue, 150 ms). Upper panel displays full chromatograms, and lower panels display styrene (left), dimer (center) and trimer (right) peaks. Solid circles indicate data points obtained from each SIM cycle. Note different ranges of axes.

Fig. 4 shows full chromatograms obtained from the SIM methods along with inset panels showing the styrene monomer, dimer, and trimer peaks. SIMA yields a very well-defined styrene peak with around 20 data points, while the SIMB and SIMC method yield 15 and 10 data points across the peak, respectively. The styrene peak is both quite broad and intense, so 20 data points is an adequate amount to define the peak. In this case, 10 data points are not adequate as the peak maximum is not well-defined. The dimer and trimer peaks are more narrow and less intense than the styrene peak and, hence, need fewer data points than the styrene peak to be well-defined. The most intense dimer and trimer peaks are obtained with SIMB with around 15 data points per peak, while the least intense dimer and trimer peaks are obtained by the SIMA method, also with around 15 data points per peak. The SIMC method yields 10 data points per peak for the dimer and trimer. The SIMA method provides very well-defined peaks, however, at the expense of intensity loss. The SIM methods provide similar SNRs for the styrene peak on the order of $10^4$. SIMA yields a SNR for the dimer peak of around one third of those obtained from the SIMB and SIMC methods. For the trimer peak, SIMA yields a SNR about half of those obtained from the SIMB and SIMC methods.

Based on the considerations of SNRs, the number of data points across a peak, and the signal intensity, the best method for the dimer and trimer peaks is SIMB. For the styrene peak the best method is SIMA. The intensity of the styrene peak is more than tenfold those of the dimer and trimer peaks. Thus, the method that results in the highest intensity of the dimer and trimer peak is preferred. The optimal dwell time is 100 ms, and the final optimized method is SIMB.

### 3.4. Calibration curve

Calibration data were obtained with the SIMB method for both ePS and 800 nm PSL standards, in the mass range of 1-230 ng and 1-85 ng, respectively. Standards were corrected with respect to instrument and procedural blanks. Calibration curves are given in Fig. 5 and regression parameters are listed in Tables 2 and 3. For styrene, a linear dependency is observed between PS mass and peak area in the 0-30 ng range. Above 30 ng, the peak area reaches a plateau and a polynomial

**Table 2**
Regression parameters obtained from linear least squares analysis for ePS and PSL calibration curves. Slope and intercept are given with the associated standard error (SE). Note that styrene parameters are obtained for the 0-30 ng mass range.

|     |         | Slope ± SE | Intercept ± SE | $R^2$ | $p$-value |
|-----|---------|-----------|----------------|-------|-----------|
| ePS | Styrene | $(4.4 \pm 0.5) \cdot 10^4$ | $(1.8 \pm 0.7) \cdot 10^5$ | 0.832 | $8.6 \cdot 10^{-9}$ |
|     | Dimer   | $122 \pm 5$ | $-254 \pm 385$ | 0.938 | $1.1 \cdot 10^{-22}$ |
|     | Trimer  | $481 \pm 27$ | $(2.9 \pm 1.9) \cdot 10^3$ | 0.903 | $2.8 \cdot 10^{-19}$ |
| PSL | Styrene | $(3.4 \pm 0.3) \cdot 10^4$ | $(7.0 \pm 5.5) \cdot 10^4$ | 0.865 | $2.4 \cdot 10^{-8}$ |
|     | Dimer   | $62 \pm 6$ | $-192 \pm 228$ | 0.812 | $1.9 \cdot 10^{-9}$ |
|     | Trimer  | $120 \pm 18$ | $793 \pm 657$ | 0.665 | $1.2 \cdot 10^{-6}$ |

**Table 3**
Regression parameters for the styrene data obtained from polynomial fits of the type $A = p1 \cdot m_{PS}^2 + p2 \cdot m_{PS} + p3$ where $A$ is the styrene peak area and $m_{PS}$ the polystyrene mass. CI denotes 95% confidence intervals.

| Coefficients | ePS | PSL |
|--------------|-----|-----|
| **p1** ± CI | $-298 \pm 82$ | $-287 \pm 90$ |
| **p2** ± CI | $(4 \pm 1) \cdot 10^4$ | $(4 \pm 1) \cdot 10^4$ |
| **p3** ± CI | $(2 \pm 1) \cdot 10^5$ | $(4 \pm 10) \cdot 10^4$ |
| **$R^2$** | 0.892 | 0.949 |

trend is observed (of the type $A = p1 \cdot m_{PS}^2 + p2 \cdot m_{PS} + p3$ where $A$ is the styrene peak area and $m_{PS}$ the polystyrene mass). The dimer and trimer peaks follow a linear trend over the entire mass range. Styrene data from the ePS calibration shows more variability than from the PSL calibration. For the dimer and trimer, the opposite is observed, where the PSL calibration data has a higher variability than the ePS data. Similar sensitivities are obtained for styrene from the two calibrations. For the dimer and trimer, higher sensitivities are obtained by the ePS calibration. The correlation coefficients ($R^2$) all exceed 0.7, i.e. the linear fits explain 70% of the variability in the data. The highest $R^2$ is obtained from the ePS dimer data with a value of 0.94, however, the standard
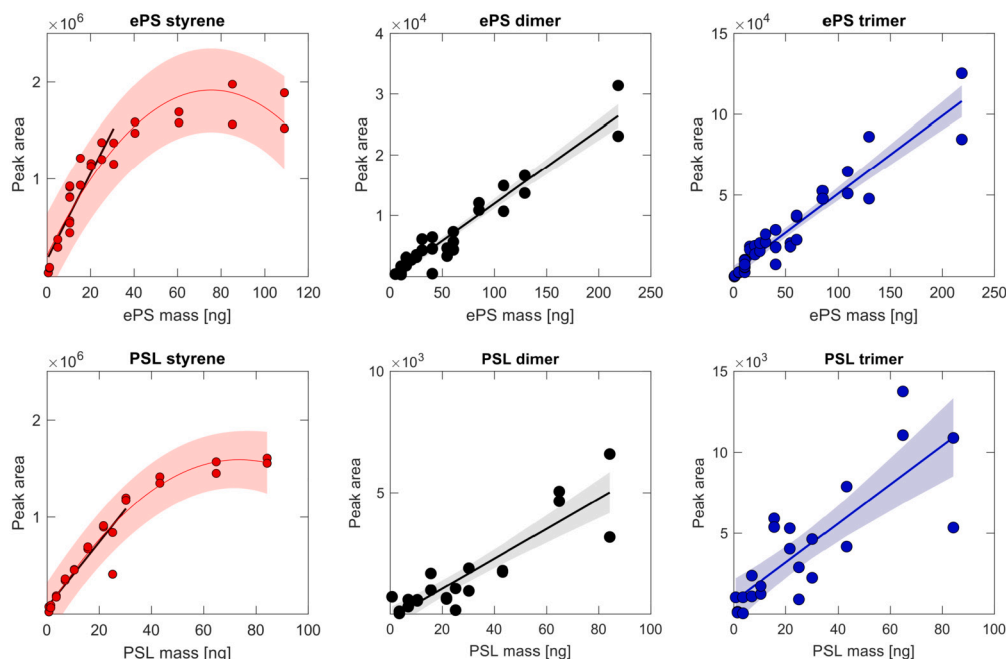
**Fig. 5.** Calibration curves of ePS (upper panels) and PSL (lower panels) based on the styrene monomer (left), dimer (center) and trimer (right). Shaded areas denote 95% confidence intervals. A linear fit to the styrene monomer data in the 0-30 ng range is given as a black line. Note different ranges for x- and y-axes.

**Table 4**
Detection and quantification limits obtained for the styrene monomer, dimer and trimer peaks for ePS and PSL based on 7 replicates of 10.4 ng standards. SD denotes the standard deviation.

|     |         | LOD ± SD [ng] | LOQ ± SD [ng] |
|-----|---------|---------------|---------------|
| ePS | Styrene | < 1           | < 1           |
|     | Dimer   | 3 ± 2         | 10 ± 7        |
|     | Trimer  | 1 ± 1         | 2 ± 2         |
|     |         |               |               |
| PSL | Styrene | < 1           | < 1           |
|     | Dimer   | 3 ± 1         | 10 ± 3        |
|     | Trimer  | 1 ± 1         | 4 ± 2         |

error of the intercept exceeds the value of the intercept. The same is seen for the PSL dimer calibration. The styrene PSL polynomial regression also yields an $R^2$ value of 0.94, however, the confidence intervals of the $p3$ coefficient exceed the value of the coefficient itself. All linear regressions show a correlation between PS mass and peak area with $p$-values $< 0.05$. Overall, the calibration curves are useful for the quantification of PS on the nanogram scale, which is the expected range for PS in aerosol samples. The ePS trimer and PSL styrene curves perform the best.

Table 4 lists the LOD and LOQ obtained from ePS and PSL for the styrene monomer, dimer, and trimer peaks. LOD and LOQ values obtained by the styrene peak are very low with values below 1 ng. The dimer peak yields values for LOD and LOQ of $3 \pm 2$ ng and $10 \pm 7$ ng, respectively, and the trimer peak yields LOD values of $1 \pm 1$ ng and LOQ values of $2 \pm 2$ ng for ePS, and $4 \pm 2$ ng for PSL. These values are lower than those previously reported by Marten and Scholz-Böttcher [58], who obtained LOD and LOQ for the styrene monomer of 3 ng and 16 ng, respectively, and LOD and LOQ of 59 ng and 282 ng for the trimer, respectively. Dimer values were not reported. For qualitative analysis of PS, the presence of the styrene monomer along with the dimer and/or the trimer is necessary in order to verify that the styrene signal arises from PS. The LOD of PS is thus limited by the LOD of the dimer and/or trimer. By using the trimer peak as a qualifier, the LOD of PS is $1 \pm 1$ ng. The validity of this low LOD is supported by the pyrograms/chromatograms obtained from ePS and PSL standards of 1 ng

where SNR for the styrene peak $> 800$ and SNR $> 5$ for the trimer peak. Ideally, the styrene peak would be used for quantitative analysis of PS, however, if other sources than PS contribute to the styrene peak it is better to use the dimer or trimer peak. Styrene pollution in ambient air has several sources e.g. styrene containing polymers (apart from PS), processing of petrochemicals [59], and biomass burning [60]. If signal from the sample matrix overlap with the dimer or trimer peaks, it is recommended to use the peak that is most well-resolved for PS quantification.

### 3.5. Validation of PS analysis in aerosol samples

In the chromatograms obtained from punch-outs of filters with low (7 μg; filter A) and high (53 μg; filter B) PM$_{2.5}$ loadings spiked with ePS, several chromatographic peaks were present in the 10-22 min RT range (see Supplementary Information Fig. 1). The styrene peak at 9 min and the trimer peak at 27 min were well-resolved, while the dimer peak at 20 min was not properly resolved due to overlapping chromatographic peaks. In order to verify the presence of ePS, both the styrene monomer along with the dimer and/or trimer need to be detected. Here, the sample matrix is not well characterized and sources of styrene other than PSL could be present. The styrene and the trimer peaks obtained from the ePS calibration were used to determine the amount of ePS on the filters. Table 5 lists the detected ePS masses on filters A and B for the different spikes. No ePS was detected on the non-spiked filters. On filter A both 20 ng and 60 ng ePS were detected with the styrene and trimer peaks.

The styrene calibration underestimates the ePS mass by a factor of 2 for the 20 ng spike and performs well for the 60 ng spike for filter A. The trimer calibration overestimates the ePS mass by a factor of $\sim 2$. A similar trend was observed for the filters with a general background contamination level from laboratory handling (data not shown). For filter B, the 20 ng ePS was not detected, neither for the styrene nor trimer peaks despite LODs $< 1$ ng. The 60 ng ePS was not detected with the trimer peak, while $4 \pm 1$ ng ePS was detected with the styrene peak.

This suggests that matrix on filter B influences the analysis, while matrices on filter A and the background contamination test filter (data not shown) only have a minor influence on the analysis. The large variability observed for the trimer from these filters (A and test) is in-

**Table 5**

Detected ePS masses on filter A (7 $\mu$g PM$_{2.5}$ per punch-out) and filter B (53 $\mu$g PM$_{2.5}$ per punch-out) obtained from the ePS calibration data for the styrene and trimer peak. TD indicates that a thermal desorption step was performed prior to pyrolysis. ND denotes not detected, and <LOQ refers to values between the LOD and LOQ.

| ePS spike [ng] | ePS detected [ng] | | | | | |
|---|---|---|---|---|---|---|
| | Styrene calibration | | | Trimer calibration | | |
| | Filter A | Filter B | Filter B TD | Filter A | Filter B | Filter B TD |
| 0 | ND | ND | ND | ND | ND | ND |
| 20 | $10 \pm 3$ | ND | $4 \pm 1$ | $34 \pm 14$ | ND | <LOQ |
| 60 | $57 \pm 17$ | $4 \pm 1$ | $19 \pm 6$ | $118 \pm 27$ | ND | $36 \pm 26$ |

stead expected to arise from the low signal intensity and sensitivity of the trimer. For filter B, the species present in the matrix may form secondary products with ePS during pyrolysis, hence minimizing the formation of styrene and the trimer resulting in low recovery of PS.

A way to minimize the matrix effect is to thermally desorb the matrix prior to pyrolysis. This was tested for filter B spiked with 20 ng and 60 ng of ePS. First, the sample was heated from $100\,°C$ to $300\,°C$ at $5\,°C\ s^{-1}$ in the pyrolyzer, and analyzed using the same oven program and MS settings as in the SIMB method to test if any ePS was lost during the thermal desorption step. Then, the same sample was pyrolyzed at $300\,°C$ to $800\,°C$ at $5\,°C\ s^{-1}$ and analyzed with the SIMB method to quantify ePS. This approach improves the detectability of ePS for both the styrene and trimer peak. For direct pyrolysis, the 20 ng spike was not detected with either of the peaks and for pyrolysis following the thermal desorption step, $4 \pm 1$ ng was detected with the styrene peak and $< 2$ ng was detected with the trimer peak. For the 60 ng spike, the styrene calibration yields $4 \pm 1$ ng for the direct pyrolysis and $19 \pm 6$ ng for pyrolysis following thermal desorption. Using the trimer peak, $36 \pm 26$ ng ePS was detected for the 60 ng spike for pyrolysis after the thermal desorption step, whereas no ePS was detected in the direct pyrolysis run.

Considering that both the styrene monomer and/or trimer need to be detected in order to verify the presence of ePS, direct pyrolysis does not allow for detection of the 20 ng and 60 ng ePS spike on filter B with high amount of aerosol matrix. The thermal desorption step prior to pyrolysis allows for detection of ePS both for the 20 ng and 60 ng spike. Semi-quantification is possible as the mass of ePS is underestimated by a factor of 3-5. This is likely due to matrix effects from components that were not desorbed at $300\,°C$. Introducing a thermal desorption step prior to pyrolysis improves the detectability of ePS in an urban PM$_{2.5}$ matrix. However, values of LOD and LOQ $< 1$ ng as obtained from the ePS standards cannot be obtained for ePS in high mass loadings of PM$_{2.5}$ matrix. In the case of low PM$_{2.5}$ loadings (for a 3-day sampling period of PM$_{2.5}$ with an average concentration of $8 \pm 3$ $\mu$g m$^{-3}$ at a flow rate of 500 L min$^{-1}$ on a 15 cm diameter filter), the LOD of $1 \pm 1$ ng as governed by the trimer peak, corresponds to a PS concentration in the air of $1 \pm 1$ ng m$^{-3}$.

The study demonstrates that the SIMB method can be used to detect ePS on the nanogram scale in an ambient aerosol matrix, but large uncertainties are associated with the quantification. Increased aerosol loadings will suppress the ePS signal, however, matrix effects can be reduced by performing a thermal desorption step prior to pyrolysis. Future work could also explore the possibility of enzymatic digestion to minimize matrix effects.

## 4. Conclusion

An optimized method for polystyrene analysis with py-GC-MS was developed using a slow temperature ramping of the pyrolysis temperature. The optimization was done with respect to the temperature of the cooled injection system, the split ratio of the cooled injection system, and the dwell time in the selected ion monitoring mode. The selection of optimal parameters was based on the styrene monomer, dimer, and trimer peak area, intensity, symmetry, signal-to-noise ratio, number of data points across chromatographic peaks, as well as the number of chromatographic peaks, and analysis time. The optimized parameters are: CIS temperature $= -40\,°C$, CIS split ratio $= 50:1$, and SIM dwell time $= 100$ ms. Calibration curves were constructed for two types of PS: expanded polystyrene and 800 nm polystyrene latex spheres. To detect PS, the styrene monomer needs to be present along with the styrene dimer and/or trimer. Thus the limit of detection was $1 \pm 1$ ng (acquired from the styrene trimer peak). The limit of quantification obtained by the styrene monomer peak was $< 1$ ng.

The method was tested for PS in an urban PM$_{2.5}$ matrix of low (7 $\mu$g per sample) and high (53 $\mu$g per sample) aerosol mass loading. The styrene calibration performs well for low aerosol loadings, while the trimer calibration overestimates the PS mass by a factor of 2. A high aerosol loading suppresses the styrene monomer and trimer signals. Introduction of a thermal desorption step prior to pyrolysis increases the detectability, however, the PS mass is still underestimated by a factor of 3-5. The method is able to detect PS on the nanogram scale in an aerosol matrix, although large uncertainties remain in the quantification. The method can be considered as a starting point for further development to include more polymers. In summary, the study presents a novel method for detection and semi-quantification of PS on the nanogram scale in atmospheric aerosol samples.

## CRediT authorship contribution statement

**Freja Hasager:** Conceptualization, Formal analysis, Investigation, Writing – original draft, Writing – review & editing, Methodology, Visualization. **Þuríður N. Björgvinsdóttir:** Formal analysis, Investigation, Writing – original draft, Writing – review & editing. **Sofie F. Vinther:** Formal analysis, Investigation, Visualization, Writing – review & editing. **Antigoni Christofili:** Formal analysis, Visualization, Writing – review & editing. **Eva R. Kjærgaard:** Conceptualization, Investigation, Writing – review & editing. **Sarah S. Petters:** Conceptualization, Methodology, Writing – review & editing. **Merete Bilde:** Conceptualization, Funding acquisition, Resources, Supervision, Writing – review & editing. **Marianne Glasius:** Conceptualization, Funding acquisition, Project administration, Resources, Supervision, Writing – original draft, Writing – review & editing.

## Declaration of competing interest

The authors declare that they have no known competing financial interests or personal relationships that could have appeared to influence the work reported in this paper.

## Data availability

Data will be made available on request.

## Acknowledgements

## Appendix A. Supplementary material

Supplementary material related to this article can be found online at https://doi.org/10.1016/j.chroma.2023.464622.

## References

[1] P.L. Corcoran, M.C. Biesinger, M. Grifi, Plastics and beaches: a degrading relationship, Mar. Pollut. Bull. 58 (1) (2009) 80–84.

[2] S. Lambert, M. Wagner, Characterisation of nanoplastics during the degradation of polystyrene, Chemosphere 145 (2016) 265–268.

[3] Y.K. Song, S.H. Hong, M. Jang, G.M. Han, S.W. Jung, W.J. Shim, Combined effects of UV exposure duration and mechanical abrasion on microplastic fragmentation by polymer type, Environ. Sci. Technol. 51 (8) (2017) 4368–4376.

[4] R.C. Thompson, Y. Olsen, R.P. Mitchell, A. Davis, S.J. Rowland, A.W.G. John, D. McGonigle, A.E. Russell, Lost at sea: where is all the plastic?, Science 304 (5672) (2004) 838.

[5] J. Brahney, M. Hallerud, E. Heim, M. Hahnenberger, S. Sukumaran, Plastic rain in protected areas of the United States, Science 368 (6496) (2020) 1257–1260.

[6] S. Yang, M. Zhou, X. Chen, L. Hu, Y. Xu, W. Fu, C. Li, A comparative review of microplastics in lake systems from different countries and regions, Chemosphere 286 (2022) 131806.

[7] M. Sajjad, Q. Huang, S. Khan, M.A. Khan, Y. Liu, J. Wang, F. Lian, Q. Wang, G. Guo, Microplastics in the soil environment: a critical review, Environ. Technol. Innov. 27 (2022) 102408.

[8] D. Materić, H.A. Kjær, P. Vallelonga, J.-L. Tison, T. Röckmann, R. Holzinger, Nanoplastics measurements in northern and southern polar ice, Environ. Res. 208 (2022) 112741.

[9] S.E. Nelms, J. Barnett, A. Brownlow, N. Davison, R. Deaville, T.S. Galloway, P.K. Lindeque, D. Santillo, B.J. Godley, Microplastics in marine mammals stranded around the British coast: ubiquitous but transitory?, Sci. Rep. 9 (1) (2019) 1075.

[10] H.A. Leslie, M.J. van Velzen, S.H. Brandsma, A.D. Vethaak, J.J. Garcia-Vallejo, M.H. Lamoree, Discovery and quantification of plastic particle pollution in human blood, Environ. Int. 163 (2022) 107199.

[11] A. Ragusa, A. Svelato, C. Santacroce, P. Catalano, V. Notarstefano, O. Carnevali, F. Papa, M.C.A. Rongioletti, F. Baiocco, S. Draghi, E. D'Amore, D. Rinaldo, M. Matta, E. Giorgini, Plasticenta: first evidence of microplastics in human placenta, Environ. Int. 146 (2021) 106274.

[12] M. Revel, A. Châtel, C. Mouneyrac, Micro(nano)plastics: a threat to human health?, Curr. Opin. Environ. Sci. Health 1 (2018) 17–23.

[13] A.A. Horton, D.K. Barnes, Microplastic pollution in a rapidly changing world: implications for remote and vulnerable marine ecosystems, Sci. Total Environ. 738 (2020) 140349.

[14] R. Dris, J. Gasperi, M. Saad, C. Mirande, B. Tassin, Synthetic fibers in atmospheric fallout: a source of microplastics in the environment?, Mar. Pollut. Bull. 104 (1) (2016) 290–293.

[15] S. Allen, D. Allen, V.R. Phoenix, G. Le Roux, P. Durántez Jiménez, A. Simonneau, S. Binet, D. Galop, Atmospheric transport and deposition of microplastics in a remote mountain catchment, Nat. Geosci. 12 (5) (2019) 339–344.

[16] S. Allen, D. Allen, F. Baladima, V. Phoenix, J. Thomas, G. Le Roux, J. Sonke, Evidence of free tropospheric and long-range transport of microplastic at Pic du Midi Observatory, Nat. Commun. 12 (1) (2021) 7242.

[17] R. Dris, J. Gasperi, C. Mirande, C. Mandin, M. Guerrouache, V. Langlois, B. Tassin, A first overview of textile fibers, including microplastics, in indoor and outdoor environments, Environ. Pollut. 221 (2017) 453–458.

[18] S. Dehghani, F. Moore, R. Akhbarizadeh, Microplastic pollution in deposited urban dust, Tehran Metropolis, Iran, Environ. Sci. Pollut. Res. Int. 24 (2017) 20360–20371.

[19] L. Cai, J. Wang, J. Peng, Z. Tan, Z. Zhan, X. Tan, Q. Chen, Characteristic of microplastics in the atmospheric fallout from Dongguan city, China: preliminary research and first evidence, Environ. Sci. Pollut. Res. Int. 24 (2017) 24928–24935.

[20] M. Bergmann, S. Mützel, S. Primpke, M.B. Tekman, J. Trachsel, G. Gerdts, White and wonderful? Microplastics prevail in snow from the Alps to the Arctic, Sci. Adv. 5 (8) (2019) eaax1157.

[21] L. Ferrero, L. Scibetta, P. Markuszewski, M. Mazurkiewicz, V. Drozdowska, P. Makuch, P. Jutrzenka-Trzebiatowska, A. Zaleska-Medynska, F. Saliu, E.D. Nilsson, E. Bolzacchini, Airborne and marine microplastics from an oceanographic survey at the Baltic Sea: an emerging role of air-sea interaction?, Sci. Total Environ. 824 (2022) 153709.

[22] X. Wang, C. Li, K. Liu, L. Zhu, Z. Song, D. Li, Atmospheric microplastic over the South China Sea and East Indian Ocean: abundance, distribution and source, J. Hazard. Mater. 389 (2020) 121846.

[23] M. Trainic, J.M. Flores, I. Pinkas, M.L. Pedrotti, F. Lombard, G. Bourdin, G. Gorsky, E. Boss, Y. Rudich, A. Vardi, et al., Airborne microplastic particles detected in the remote marine atmosphere, Commun. Earth Environ. 1 (1) (2020) 64.

[24] M. González-Pleiter, C. Edo, Ángeles Aguilera, D. Viúdez-Moreiras, G. Pulido-Reyes, E. González-Toril, S. Osuna, G. de Diego-Castilla, F. Leganés, F. Fernández-Piñas, R. Rosal, Occurrence and transport of microplastics sampled within and above the planetary boundary layer, Sci. Total Environ. 761 (2021) 143213.

[25] N. Evangeliou, H. Grythe, Z. Klimont, C. Heyes, S. Eckhardt, S. Lopez-Aparicio, A. Stohl, Atmospheric transport is a major pathway of microplastics to remote regions, Nat. Commun. 11 (1) (2020) 3381.

[26] J. Brahney, N. Mahowald, M. Prank, G. Cornwell, Z. Klimont, H. Matsui, K.A. Prather, Constraining the atmospheric limb of the plastic cycle, Proc. Natl. Acad. Sci. 118 (16) (2021) e2020719118.

[27] S. Allen, D. Allen, K. Moss, G. Le Roux, V.R. Phoenix, J.E. Sonke, Examination of the ocean as a source for atmospheric microplastics, PLoS ONE 15 (5) (2020) e0232746.

[28] L.E. Revell, P. Kuma, E.C. Le Ru, W.R. Somerville, S. Gaw, Direct radiative effects of airborne microplastics, Nature 598 (7881) (2021) 462–467.

[29] S.-J. Royer, S. Ferrón, S.T. Wilson, D.M. Karl, Production of methane and ethylene from plastic in the environment, PLoS ONE 13 (8) (2018) e0200574.

[30] M. Kozjek, D. Vengust, T. Radošević, G. Žitko, S. Koren, N. Toplak, I. Jerman, M. Butala, M. Podlogar, M.K. Viršek, Dissecting giant hailstones: a glimpse into the troposphere with its diverse bacterial communities and fibrous microplastics, Sci. Total Environ. 856 (2023) 158786.

[31] M. Aeschlimann, G. Li, Z.A. Kanji, D.M. Mitrano, Potential impacts of atmospheric microplastics and nanoplastics on cloud formation processes, Nat. Geosci. (2022) 1–9.

[32] G. Renner, T.C. Schmidt, J. Schram, Analytical methodologies for monitoring micro(nano)plastics: which are fit for purpose?, Curr. Opin. Environ. Sci. Health 1 (2018) 55–61.

[33] S. Abbasi, B. Keshavarzi, F. Moore, A. Turner, F.J. Kelly, A.O. Dominguez, N. Jaafarzadeh, Distribution and potential health impacts of microplastics and microrubbers in air and street dusts from Asaluyeh County, Iran, Environ. Pollut. 244 (2019) 153–164.

[34] J. La Nasa, G. Biale, D. Fabbri, F. Modugno, A review on challenges and developments of analytical pyrolysis and other thermoanalytical techniques for the quali-quantitative determination of microplastics, J. Anal. Appl. Pyrolysis 149 (2020) 104841.

[35] L.Y. Vélez-Escamilla, F.F. Contreras-Torres, Latest advances and developments to detection of micro- and nanoplastics using surface-enhanced Raman spectroscopy, Part. Part. Syst. Charact. 39 (3) (2022) 2100217.

[36] D. Materić, A. Kasper-Giebl, D. Kau, M. Anten, M. Greilinger, E. Ludewig, E. van Sebille, T. Röckmann, R. Holzinger, Micro- and nanoplastics in Alpine snow: a new method for chemical identification and (semi)quantification in the nanogram range, Environ. Sci. Technol. 54 (4) (2020) 2353–2359.

[37] V.K. Sharma, X. Ma, E. Lichtfouse, D. Robert, Nanoplastics are potentially more dangerous than microplastics, Environ. Chem. Lett. (2022) 1–4.

[38] D. Materić, E. Ludewig, D. Brunner, T. Röckmann, R. Holzinger, Nanoplastics transport to the remote, high-altitude Alps, Environ. Pollut. 288 (2021) 117697.

[39] Y. Zhang, S. Kang, S. Allen, D. Allen, T. Gao, M. Sillanpää, Atmospheric microplastics: a review on current status and perspectives, Earth-Sci. Rev. 203 (2020) 103118.

[40] L. Hermabessiere, C. Himber, B. Boricaud, M. Kazour, R. Amara, A.-L. Cassone, M. Laurentie, I. Paul-Pont, P. Soudant, A. Dehaut, et al., Optimization, performance, and application of a pyrolysis-GC/MS method for the identification of microplastics, Anal. Bioanal. Chem. 410 (25) (2018) 6663–6676.

[41] D. Fabbri, A.G. Rombolà, I. Vassura, C. Torri, S. Franzellitti, M. Capolupo, E. Fabbri, Off-line analytical pyrolysis GC–MS to study the accumulation of polystyrene microparticles in exposed mussels, J. Anal. Appl. Pyrolysis 149 (2020) 104836.

[42] E. Fries, J.H. Dekiff, J. Willmeyer, M.-T. Nuelle, M. Ebert, D. Remy, Identification of polymer types and additives in marine microplastic particles using pyrolysis-GC/MS and scanning electron microscopy, Environ. Sci. Process. Impacts 15 (10) (2013) 1949–1956.

[43] S. Tsuge, H. Ohtani, C. Watanabe, Pyrolysis-GC/MS Data Book of Synthetic Polymers: Pyrograms, Thermograms and MS of Pyrolyzates, Elsevier, 2011.

[44] I. Coralli, V. Giorgi, I. Vassura, A.G. Rombolà, D. Fabbri, Secondary reactions in the analysis of microplastics by analytical pyrolysis, J. Anal. Appl. Pyrolysis 161 (2022) 105377.

[45] J. Whitecavage, J.R. Stuff, L. Vernarelli, Determination of microplastics using pyrolysis gas chromatography mass spectrometry, Gerstel Appl. Note (2020).

[46] R. Geyer, J.R. Jambeck, K.L. Law, Production, use, and fate of all plastics ever made, Sci. Adv. 3 (7) (2017) e1700782.

[47] K. Liu, T. Wu, X. Wang, Z. Song, C. Zong, N. Wei, D. Li, Consistent transport of terrestrial microplastics to the ocean through atmosphere, Environ. Sci. Technol. 53 (18) (2019) 10612–10619.

[48] J. Reichel, J. Graßmann, T. Letzel, J.E. Drewes, Systematic development of a simultaneous determination of plastic particle identity and adsorbed organic compounds by thermodesorption–pyrolysis GC/MS (TD-Pyr-GC/MS), Molecules 25 (21) (2020) 4985.

[49] J.M. Miller, Chromatography: Concepts and Contrasts, 2nd edition, John Wiley & Sons, 2009.

[50] T. Ellermann, C. Nordstrøm, A. Massling, M.B. Sørensen, Status for Måling af Luftkvalitet i 2022 (status for measuring air quality in 2022), Aarhus University, DCE - Danish Centre for Environment and Energy, 2023.

[51] D.M.I. DMI, Weather archive, https://www.dmi.dk/vejrarkiv/. (Accessed 9 February 2023).

[52] The Mathworks, Inc., Natick, Massachusetts, 2021, MATLAB version 9.10.0.1739362 (R2021a).

[53] H. Ohtani, T. Yuyama, S. Tsuge, B. Plage, H.-R. Schulten, Study on thermal degradation of polystyrenes by pyrolysis-gas chromatography and pyrolysis-field ionization mass spectrometry, Eur. Polym. J. 26 (8) (1990) 893–899.

[54] T. Faravelli, M. Pinciroli, F. Pisano, G. Bozzano, M. Dente, E. Ranzi, Thermal degradation of polystyrene, J. Anal. Appl. Pyrolysis 60 (1) (2001) 103–121.

[55] R.A. Meyers, Encyclopedia of Physical Science and Technology, Academic Press, 2002.

[56] D. Matthews, J. Hayes, Systematic errors in gas chromatography-mass spectrometry isotope ratio measurements, Anal. Chem. 48 (9) (1976) 1375–1382.

[57] J.D. Pleil, T.L. Vossler, W.A. McClenny, K.D. Oliver, Optimizing sensitivity of SIM mode of GC/MS analysis for EPA's TO-14 air toxics method, J. Air Waste Manage. Assoc. 41 (3) (1991) 287–293.

[58] M. Fischer, B.M. Scholz-Böttcher, Microplastics analysis in environmental samples – recent pyrolysis-gas chromatography-mass spectrometry method improvements to increase the reliability of mass-related data, Anal. Methods 11 (18) (2019) 2489–2497.

[59] W.B. Knighton, S.C. Herndon, E.C. Wood, E.C. Fortner, T.B. Onasch, J. Wormhoudt, C.E. Kolb, B.H. Lee, M. Zavala, L. Molina, M. Jones, Detecting fugitive emissions of 1, 3-butadiene and styrene from a petrochemical facility: an application of a mobile laboratory and a modified proton transfer reaction mass spectrometer, Ind. Eng. Chem. Res. 51 (39) (2012) 12706–12711.

[60] G. Barrefors, G. Petersson, Assessment by gas chromatography and gas chromatography-mass spectrometry of volatile hydrocarbons from biomass burning, J. Chromatogr. A 710 (1) (1995) 71–77.